

## Dynamics of localized waves in a $(3 + 1)$ -dimensional nonlinear evolution equation

Yunfei Yue<sup>\*,†</sup> and Yong Chen<sup>\*,†,‡,§</sup>

*\*Institute of Computer Theory,  
East China Normal University, Shanghai 200062, China*  
*†Shanghai Key Laboratory of Trustworthy Computing,  
East China Normal University, Shanghai 200062, China*  
*‡Department of Physics, Zhejiang Normal University,  
Jinhua 321004, China*  
*§ychen@sei.ecnu.edu.cn*

Received 17 November 2018

Accepted 26 December 2018

Published 13 March 2019

In this paper, a  $(3 + 1)$ -dimensional nonlinear evolution equation is studied via the Hirota method. Soliton, lump, breather and rogue wave, as four types of localized waves, are derived. The obtained  $N$ -soliton solutions are dark solitons with some constrained parameters. General breathers, line breathers, two-order breathers, interaction solutions between the dark soliton and general breather or line breather are constructed by choosing suitable parameters on the soliton solution. By the long wave limit method on the soliton solution, some new lump and rogue wave solutions are obtained. In particular, dark lumps, interaction solutions between dark soliton and dark lump, two dark lumps are exhibited. In addition, three types of solutions related with rogue waves are also exhibited including line rogue wave, two-order line rogue waves, interaction solutions between dark soliton and dark lump or line rogue wave.

*Keywords:* Hirota bilinear method;  $(3 + 1)$ -dimensional nonlinear evolution equation; rogue wave; lump; breather; interaction solution.

### 1. Introduction

Studied here is a  $(3 + 1)$ -dimensional nonlinear evolution equation:

$$3u_{xz} - (2u_t + u_{xxx} - 2uu_x)_y + 2(u_x \partial_x^{-1} u_y)_x = 0. \quad (1)$$

It was proposed during the research of Algebraic-geometrical solutions by Geng.<sup>1</sup> Since then, lots of researchers have paid attentions to it. In Ref. 2,  $N$ -soliton solution expressed by Wronskian form was constructed. In Ref. 3, resonant solution and

<sup>§</sup>Corresponding author.

complexion solution were derived by virtue of the  $N$ -fold Darboux transformation (DT) of the AKNS spectral problems. In Ref. 4, rational solutions were explicitly derived by the constructed bilinear Bäcklund transformation (BT). In Ref. 5, rational solutions and rogue waves to Eq. (1) were obtained based on the procedure of a symbolic computation method. In Ref. 6, the Bell-polynomial approach was applied to seek the integrable properties of (1) and some exact solutions were derived with the help of line superposition principle and homoclinic test method. In Refs. 7–9, multiple front wave solutions were studied for the models related with Eq. (1) via Hirota’s method and Cole–Hopf transformation. In Ref. 10, Eq. (1) was verified Painlevé integrable and  $\Phi$ -integrable. In Ref. 11, multiple exp-function approach was applied to this equation for constructing multiple wave solutions and the elastic interaction behavior of solitons was explored. In Ref. 12, multi-soliton solutions were investigated by the homoclinic test method and the three-wave approach. In Ref. 13, interaction solutions were gained which showed that a lump was swallowed by a stipe. In Ref. 14, two types of resonant multiple wave solutions were obtained based on the linear superposition principle. In Ref. 15, general higher-order rogue waves were obtained by Hirota method. In Ref. 16, diversity of exact solutions was studied by the test function approach and the Hirota bilinear method.  $M$ -lump solutions and mixed lump-soliton solutions were obtained in Refs. 17 and 18.

It is not difficult to trace a strong line between Eq. (1) and the noted KdV equation. Let

$$x \rightarrow \sqrt{3}x, \quad t \rightarrow 6\sqrt{3}t, \quad u \rightarrow u.$$

The main term  $2u_t + u_{xxx} - 2uu_x$  of Eq. (1) can be transformed to the KdV equation. In addition, if setting  $y = x, z = t$  under appropriate scaling transformation,

$$x \rightarrow \frac{1}{2}x, \quad t \rightarrow -\frac{1}{8}t, \quad u \rightarrow 6u.$$

Equation (1) is also transformed to the KdV equation. As an extension of the KdV equation, Eq. (1) might be applied to pattern shallow water waves and short waves in nonlinear dispersive media.

To illustrate some physical phenomena further, it becomes more and more important to construct explicit solutions and interaction solutions among nonlinear waves. In the past years, many approaches have been developed to obtain exact solutions for nonlinear evolution equations, such as BT,<sup>19</sup> the Inverse Scattering transformation (IST),<sup>20,21</sup> DT,<sup>22,23</sup> Lie symmetry approach,<sup>24–31</sup> Hirota bilinear method<sup>32,33</sup> and so on. For a given nonlinear system, Hirota method is an effective and direct method to seek the corresponding explicit solutions. Soliton,<sup>34,35</sup> lump,<sup>36–41</sup> breather<sup>42–46</sup> and rogue wave,<sup>47–59</sup> as four types of localized wave solutions, have attracted particular attentions in both theories and experiments.

Under the following transformation

$$u = -3(\ln f)_{xx} = -3\frac{f_{xx}}{f} + 3\frac{f_x^2}{f^2}, \tag{2}$$

Equation (1) is sent to the following bilinear form:

$$(3D_x D_z - 2D_y D_t - D_x^3 D_y)(f \cdot f) = 0, \tag{3}$$

where  $f = f(x, y, z, t)$ ,  $D_x^3 D_y$ ,  $D_x D_z$  and  $D_t D_y$  are bilinear derivative operators<sup>32</sup> with

$$D_x^\alpha D_y^\beta D_z^\gamma D_t^\delta (f \cdot g) = \left(\frac{\partial}{\partial x} - \frac{\partial}{\partial x'}\right)^\alpha \left(\frac{\partial}{\partial y} - \frac{\partial}{\partial y'}\right)^\beta \left(\frac{\partial}{\partial z} - \frac{\partial}{\partial z'}\right)^\gamma \left(\frac{\partial}{\partial t} - \frac{\partial}{\partial t'}\right)^\delta \times f(x, y, z, t)g(x', y', z', t') \Big|_{x'=x, y'=y, z'=z, t'=t}. \tag{4}$$

The goal of this paper is to study four types of localized waves and interaction solutions among localized waves to Eq. (1) by virtue of the method applied in Refs. 60 and 64. The reminder of the paper is constructed as follows.  $N$ -soliton solution is derived according to Hirota approach in Sec. 2. Then it follows three kinds of localized waves by taking complex conjugate of the parameters and long wave limit on the  $N$ -soliton solution. Some cases of interaction solutions are also investigated. The last section is a short conclusion.

## 2. Localized Wave and Interaction Solutions

### 2.1. The $N$ -soliton solution

With the aid of Hirota bilinear method, we first derive  $N$ -order soliton solution of Eq. (1), which can be obtained by substituting

$$f = \sum_{\mu=0,1} \exp\left(\sum_{i=1}^N \mu_i \eta_i + \sum_{1 \leq i < j}^N \mu_i \mu_j \ln(A_{ij})\right) \tag{5}$$

into Eq. (2) via the Hirota direct method, and

$$\omega_i = -\frac{k_i^2 p_i - 3q_i}{2p_i}, \quad \eta_i = k_i(x + p_i y + q_i z + \omega_i t) + \eta_i^0, \tag{6}$$

$$A_{ij} = \frac{(k_i(k_i - k_j)p_j + q_j)p_i^2 - ((k_i - k_j)k_j p_j + q_j + q_i)p_j p_i + p_j^2 q_i}{(k_i(k_i + k_j)p_j + q_j)p_i^2 + ((k_i + k_j)k_j p_j - q_j - q_i)p_j p_i + p_j^2 q_i} \tag{6}$$

$$(i, j = 1, 2, \dots, N),$$

where  $k_i$ ,  $p_i$ ,  $q_i$  and  $\eta_i^0$  are arbitrary constants,  $\sum_{\mu=0,1}$  is the summation with possible combinations of  $\eta_i, \eta_j = 0, 1 (i, j = 1, 2, \dots, N)$ .

To demonstrate the dynamic behavior of the soliton solution, we take  $N = 1, 2, 3$  for example. It is assumed that

$$f = 1 + \exp^{\eta_1},$$

$$f = 1 + \exp^{\eta_1} + \exp^{\eta_2} + A_{12} \exp^{\eta_1 + \eta_2}, \tag{7}$$

$$f = 1 + \exp^{\eta_1} + \exp^{\eta_2} + \exp^{\eta_3} + A_{12} \exp^{\eta_1 + \eta_2} + A_{13} \exp^{\eta_1 + \eta_3} + A_{23} \exp^{\eta_2 + \eta_3} + A_{12} A_{13} A_{23} \exp^{\eta_1 + \eta_2 + \eta_3},$$

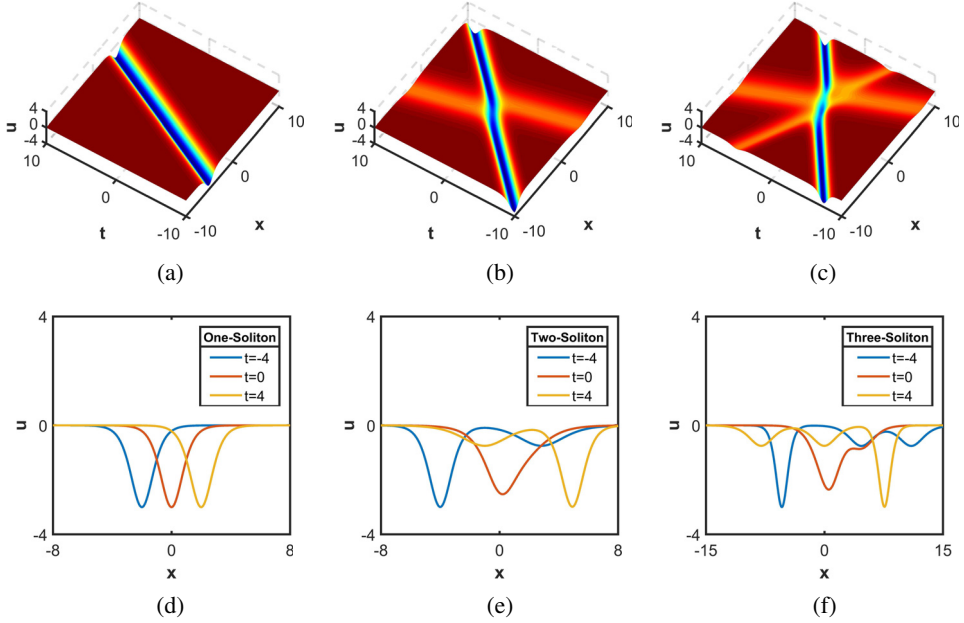


Fig. 1. (Color online) Three examples of dark soliton solutions of Eq. (1) at the  $(x, t)$  plane with parameters in Eq. (9). Up rows: three dimension graphs of soliton solutions; Down rows: the propagation of solitons over time.

with the parameters in accordance with Eq. (6). Then the dynamic behavior can be demonstrated with the following parameters:

$$\begin{aligned}
 N = 1, \quad k = 2, \quad p = 1, \quad q = 1, \quad \eta_1^0 = 0; \\
 N = 2, \quad k_1 = 1, \quad k_2 = 2, \quad q_1 = 1, \quad q_2 = 2, \quad p_1 = 2, \quad p_2 = 3, \quad \eta_1^0 = \eta_2^0 = 0; \\
 N = 3, \quad k_1 = 1, \quad k_2 = 2, \quad k_3 = 1, \quad q_1 = 2, \quad q_2 = 1, \quad q_3 = 2, \quad p_1 = 1.2, \quad (8) \\
 p_2 = 2.3, \quad p_3 = 3.3, \quad \eta_1^0 = \eta_2^0 = \eta_3^0 = 0.
 \end{aligned}$$

It is visually shown that these solutions are dark solitons and the collisions are elastic, which can be seen from Fig. 1. The small-amplitude solitons propagate fast than the large-amplitude ones. After the collision of the dark solitons, their speeds and shapes do not change, but the phases have a change.

### 2.2. The breather solutions

By taking complex conjugate approach on the soliton solutions, we will derive analytical expressions of breather solutions for Eq. (1). In different planes, the breathers can exhibit different dynamical characteristics.

In the case of  $N = 2$ , let the parameters in Eq. (5) satisfy the following constraints:

$$k_1 = k_2^* = aI, \quad q_1 = q_2 = b, \quad p_1 = p_2^* = c + dI. \quad (9)$$

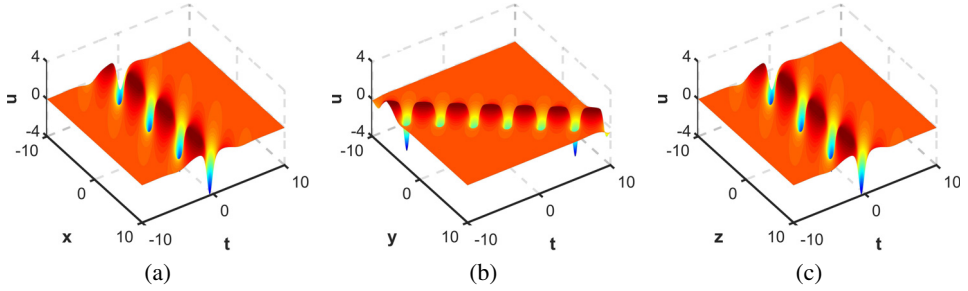


Fig. 2. (Color online) Breathers of Eq. (1) in three different planes with parameters constrained by  $a = b = c = d = 1, \eta_1^0 = \eta_2^0 = 0$ : (a)  $(x, t)$  plane, (b)  $(y, t)$  plane and (c)  $(z, t)$  plane.

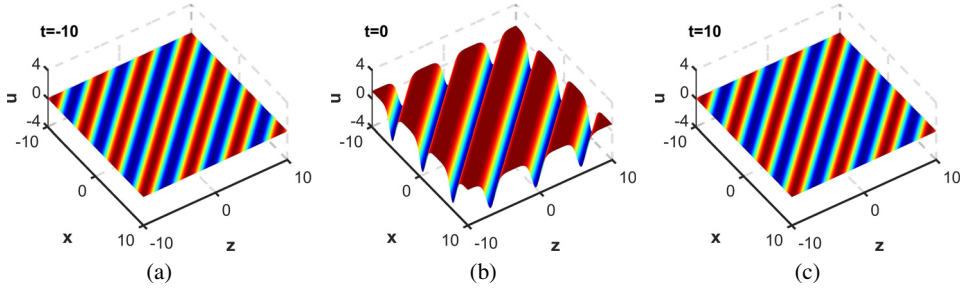


Fig. 3. (Color online) Line breathers of Eq. (1) in the  $(x, z)$  plane at  $y = 0$ . The parameters are the same as in Fig. 2.

Now  $f$  in Eq. (5) can be restated as

$$\begin{aligned}
 f = & 1 + \left( 1 + \frac{a^2 c^3 + a^2 c d^2}{b d^2} \right) \exp \left( -2 a d y + \frac{3 a b d t}{c^2 + d^2} \right) \\
 & + \exp \left( I a \left( x + (c + I d) y + \frac{1}{2} \left( a^2 + \frac{3 b}{c + I d} \right) t + b z \right) \right) \\
 & + \exp \left( -I a \left( x + (c - I d) y + \frac{1}{2} \left( a^2 + \frac{3 b}{c - I d} \right) t + b z \right) \right). \quad (10)
 \end{aligned}$$

Then, the general breathers can be derived by choosing suitable parameters in Eq. (9), whose dynamical behavior is demonstrated in Fig. 2. In the  $(x, t)$  and  $(z, t)$  planes, these breathers have the same period. They are both localized in time directions, and periodic in space directions, while in  $(y, t)$  plane, the breather is a quasi-breather, which propagates in the angular bisector of the coordinates. Based on the same parameter conditions, the line breather in the  $(x, z)$  plane can be constructed, whose global dynamic behavior is demonstrated in Fig. 3. These periodic line waves are line breathers, whose limiting cases can generate the fundamental line rogue waves. The line breather begins at a constant background to the maximum amplitude 2.9996 at  $t = 0$ . Finally, it damps to the original background.

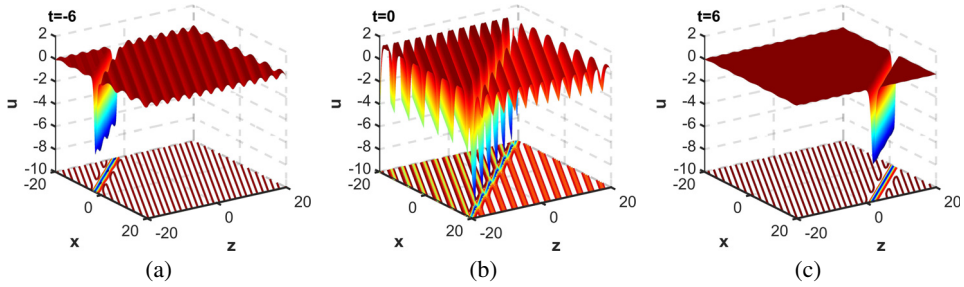


Fig. 4. (Color online) The spatial structure of interaction solution between dark soliton and line breather in  $(x, z)$  plane at  $y = 0$ . The parameters are constrained in Eq. (11).

In the case of  $N = 3$ , we would like to derive interaction solutions between solitons and breathers in six different planes by choosing suitable parameters. Without loss of generality, with the choices of the parameters

$$\begin{aligned}
 N = 3, \quad k_1 = k_3^* = I, \quad p_1 = p_3^* = 2 + 3I, \quad q_1 = q_3 = 2, \\
 k_2 = 3, \quad p_2 = 2, \quad q_2 = 1, \quad \eta_1^0 = \eta_2^0 = \eta_3^0 = 0,
 \end{aligned}
 \tag{11}$$

it can be added that

$$\begin{aligned}
 f = 1 + \exp\left(3x + 6y - \frac{45}{4}t + 3z\right) + \frac{22}{9} \exp\left(-6y + \frac{18}{3}t\right) \\
 + 2 \exp\left(-3y + \frac{9}{13}t\right) \cos\left(x + 2y + \frac{25}{26}t + 2z\right) + \frac{30206}{1989} \exp\left(3x - \frac{513}{52}t + 3z\right) \\
 + \frac{31944}{6409} \exp\left(3x + 3y - \frac{549}{52} + 3z\right) \sin\left(x + 2y + \frac{25}{26}t + 2z\right) \\
 - \frac{574}{6409} \exp\left(3x + 3y - \frac{549}{52}t + 3z\right) \cos\left(x + 2y + \frac{25}{26}t + 2z\right).
 \end{aligned}
 \tag{12}$$

Then, the interaction phenomena can be seen in Figs. 4 and 5. Obviously, the six planes own different dynamical behavior and physical phenomena, especially in the  $(x, z)$  plane. The periods and propagation directions of these interaction solutions are distinct with each other. From Fig. 4, it can be seen that the amplitude of the interaction solution reaches maximum 9.3143 at  $t = 0$ . The soliton divides the background periodic wave into two parts, and the amplitude of the left part is obviously greater than the right part's. Over time, the line breather disappears and soliton will be left alone.

In the case of  $N = 4$ , interaction solutions between breathers are constructed with the choices of suitable parameters. The function  $f$  in the four soliton solution  $u$  for Eq. (1) has the following form:

$$\begin{aligned}
 f = 1 + \exp^{\eta_1} + \exp^{\eta_2} + \exp^{\eta_3} + \exp^{\eta_4} + A_{12} \exp^{\eta_1 + \eta_2} + A_{13} \exp^{\eta_1 + \eta_3} \\
 + A_{14} \exp^{\eta_1 + \eta_4} + A_{23} \exp^{\eta_2 + \eta_3} + A_{24} \exp^{\eta_2 + \eta_4} + A_{34} \exp^{\eta_3 + \eta_4}
 \end{aligned}$$

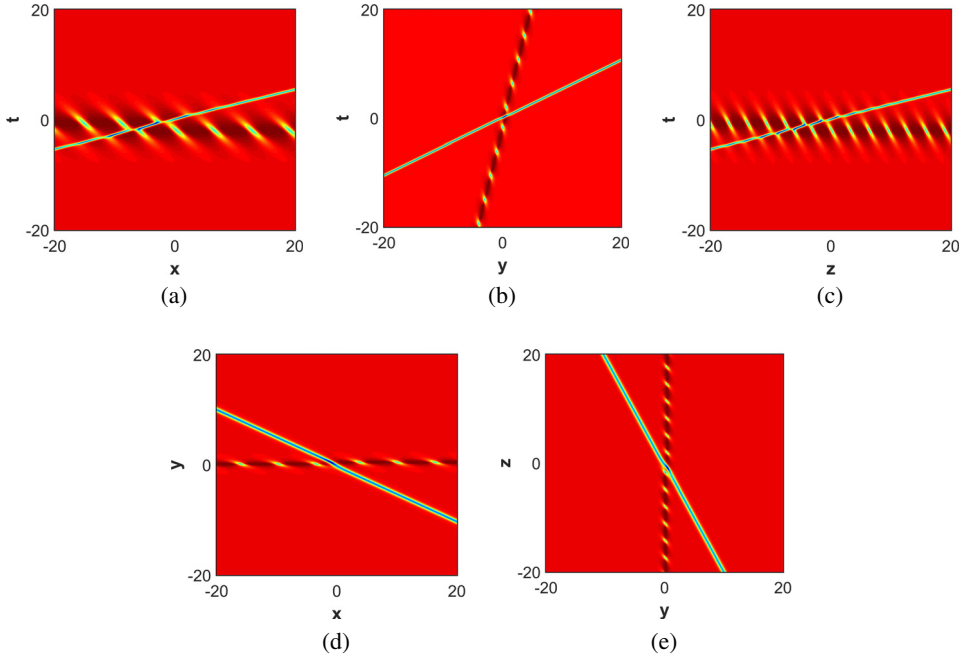


Fig. 5. (Color online) The spatial structure of interaction solution between dark soliton and general breathers in different planes. The parameters are constrained in Eq. (11).

$$\begin{aligned}
 &+ A_{12}A_{13}A_{23} \exp^{\eta_1+\eta_2+\eta_3} + A_{12}A_{14}A_{24} \exp^{\eta_1+\eta_2+\eta_4} + A_{13}A_{14}A_{34} \exp^{\eta_1+\eta_3+\eta_4} \\
 &+ A_{23}A_{24}A_{34} \exp^{\eta_2+\eta_3+\eta_4} + A_{12}A_{13}A_{14}A_{23}A_{24}A_{34} \exp^{\eta_1+\eta_2+\eta_3+\eta_4}, \quad (13)
 \end{aligned}$$

with the parameters in accordance with Eq. (6). Let the parameters in Eq. (5) as follows:

$$\begin{aligned}
 k_1 = k_2^* = I, \quad k_3 = k_4^* = 2I, \quad p_1 = p_2^* = 1 + I, \quad p_3 = p_4^* = 2 + I, \\
 q_1 = q_2 = 1, \quad q_3 = q_4 = 2, \quad \eta_i^0 = 0 \quad (i = 1, 2, 3, 4). \quad (14)
 \end{aligned}$$

It thus follows

$$\begin{aligned}
 f = &1 + 3 \exp\left(\frac{3}{2}t - 2y\right) + 21 \exp\left(\frac{12}{5}t - 4y\right) + \frac{68607}{3169} \exp\left(\frac{39}{10}t - 6y\right) \\
 &+ 2 \exp\left(\frac{3}{4}t - y\right) \cos\left(x + y + z + \frac{5}{4}t\right) + \frac{1}{117253} \exp\left(\frac{27}{10}t - 4y\right) \\
 &\times \left(352638 \cos\left(2x + 4y + 4z + \frac{32}{5}t\right) + 213840 \sin\left(2x + 4y + 4z + \frac{32}{5}t\right)\right) \\
 &+ \frac{1}{3169} \exp\left(\frac{39}{20}t - 3y\right) \left(1210 \cos\left(3x + 5y + 5z + \frac{153}{20}t\right)\right. \\
 &\left.+ 264 \sin\left(3x + 5y + 5z + \frac{153}{20}t\right)\right) + \frac{1}{117253} \exp\left(\frac{63}{20}t - 5y\right)
 \end{aligned}$$

$$\begin{aligned}
 & \times \left( 2867634 \cos \left( x + y + z + \frac{5}{4}t \right) - 332640 \sin \left( x + y + z + \frac{5}{4}t \right) \right) \\
 & + \frac{1}{37} \exp \left( \frac{39}{20}t - 3y \right) \left( 210 \cos \left( x + 3y + 3z + \frac{103}{20}t \right) \right. \\
 & \left. + 72 \sin \left( x + 3y + 3z + \frac{103}{20}t \right) \right) + 2 \exp \left( \frac{6}{5}t - 2y \right) \\
 & \times \cos \left( 2x + 4y + 4z + \frac{32}{5}t \right), \tag{15}
 \end{aligned}$$

then two kinds of two-order breathers can be derived, which are demonstrated in Figs. 6–8. In Figs. 6 and 7, the breathers are two general breathers interacting with each other. For the general breathers, the amplitudes reach maximum values 5.6334 and 4.8569. In Fig. 8, the breathers are two-line breathers. During the propagation, the two line breathers appear from a constant plane and then damp to the original plane and the amplitude reaches to the maximum 5.5309 at  $t = 0$ . The collision processes of the two type breathers are elastic.

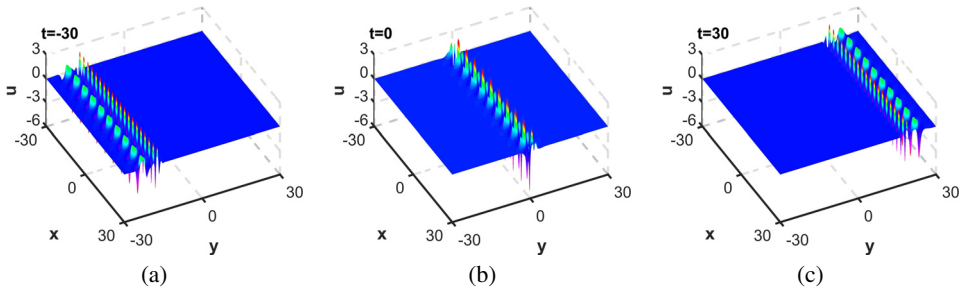


Fig. 6. (Color online) Elastic collision of two general breathers in  $(x, y)$  plane. Parameters are given in Eq. (14).

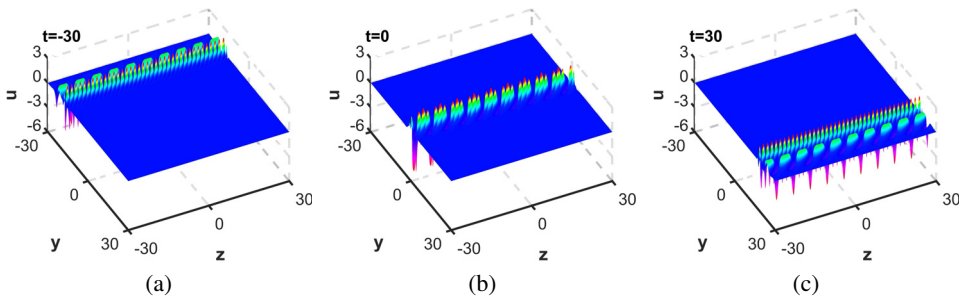


Fig. 7. (Color online) Elastic collision of two general breathers in  $(x, y)$  plane. Parameters are given in Eq. (14).

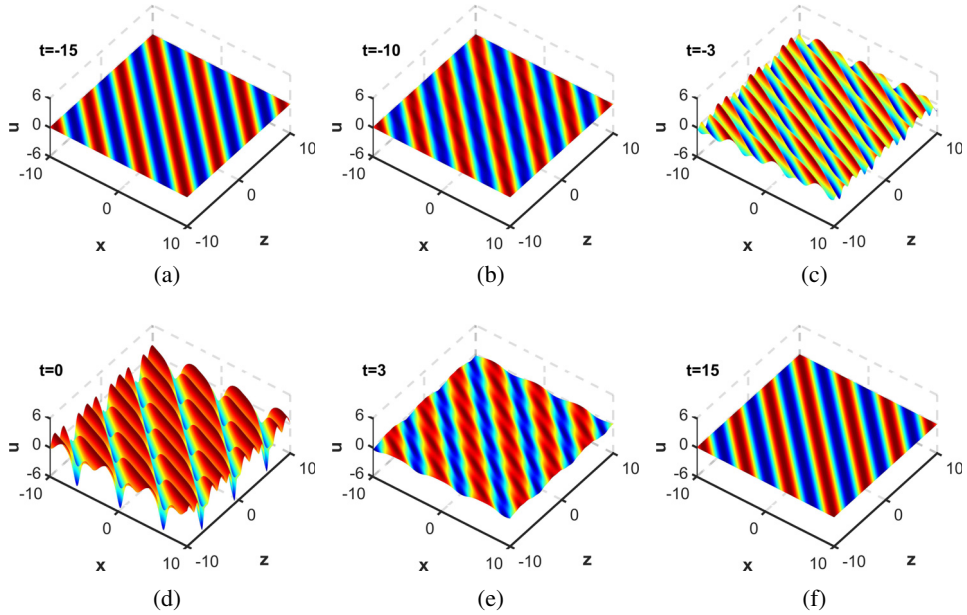


Fig. 8. (Color online) Elastic collision of two line breathers in  $(x, z)$  plane. Parameters are given in Eq. (14).

### 2.3. The lump solutions

With the long wave limit method<sup>65,66</sup> on multi-soliton solution, the lump solutions will be derived with choosing suitable parameters. In the case of  $N = 2$ , we can give the lump solution with appropriate parameters in Eq. (5) as follows:

$$N = 2, \quad k_1 = l_1\epsilon, \quad k_2 = l_2\epsilon, \quad \eta_1^0 = \eta_2^{0*} = I\pi, \quad (16)$$

it thus transpires that

$$f = (\theta_1\theta_2 + \theta_0)l_1l_2\epsilon^2 + O(\epsilon^3). \quad (17)$$

By taking the limit of  $\epsilon \rightarrow 0$  in Eq. (17), it follows

$$u = \frac{3(\theta_1^2 + \theta_2^2 - 2\theta_0)}{(\theta_1\theta_2 + \theta_0)^2} \quad (18)$$

with

$$\theta_0 = -\frac{2p_2p_1(p_1 + p_2)}{(p_1 - p_2)(p_1q_2 - p_2q_1)}, \quad (19)$$

$$\theta_i = x + p_iy + q_iz + \frac{3q_it}{2p_i} \quad (i = 1, 2).$$

By setting  $p_2 = p_1^*, q_2 = q_1^*$ , it is obvious that the rational solution  $u$  in Eq. (18) is nonsingular. Without loss of generality, we assume that  $p_1 = a_1 + Ib_1, q_1 = a_2 + Ib_2$  and  $a_1, a_2, b_1, b_2$  are all real constants in Eq. (18).

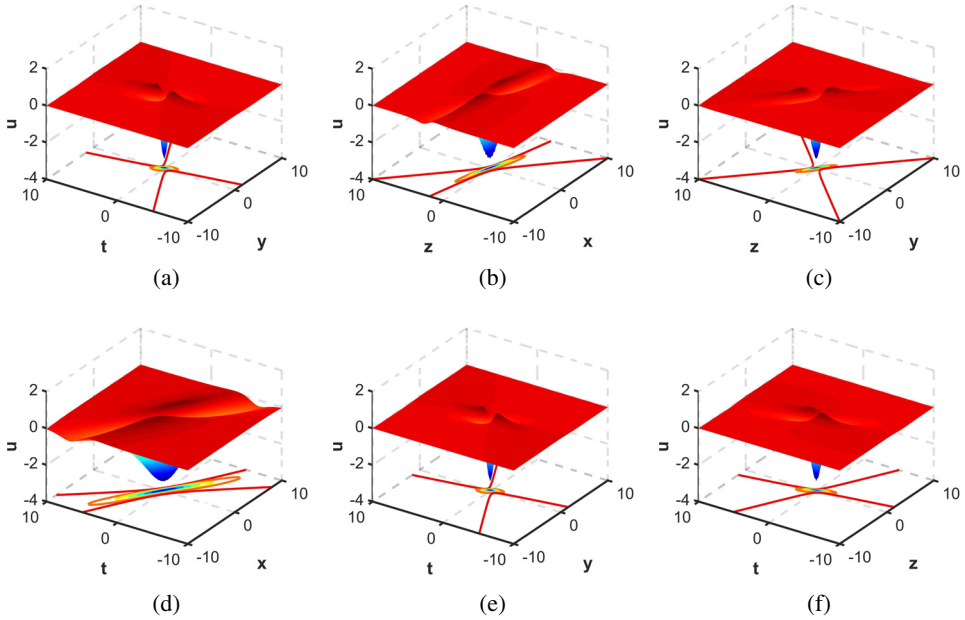


Fig. 9. (Color online) The dark lump solutions in different planes with  $a_1 = b_2 = 2, a_2 = b_1 = 3$  in Eq. (18).

When  $a_1 \neq 0$ , the trajectory can be defined along the path  $[x(t), y(t)]$  as follows:

$$\begin{aligned}
 x + a_1 y + a_2 z + \frac{3(a_1 a_2 + b_1 b_2)}{2(a_1^2 + b_1^2)} t &= 0, \\
 b_1 y + b_2 z + \frac{3(a_1 b_2 - a_2 b_1)}{2(a_1^2 + b_1^2)} t &= 0,
 \end{aligned}
 \tag{20}$$

it can be added that the solution  $u$  in Eq. (18) is a constant and keeps the permanent lump conditions in the process of propagations. By selecting suitable parameters, we can derive dark lumps in six different planes, which are visually demonstrated in Fig. 9 and localized in all directions.

In the case of  $N = 3$ , we derive interaction solutions between solitons and lumps in different planes by applying the long wave limit approach on the three-soliton solution. To demonstrate these nonsingular interaction solutions, we first constraint the parameters similar in Eq. (16),

$$N = 3, \quad k_1 = l_1 \epsilon, \quad k_2 = l_2 \epsilon, \quad k_3 = k_3, \quad \eta_1^0 = \eta_2^{0*} = I\pi, \quad \eta_3^0 = \eta_3^0, \tag{21}$$

and a suitable limit of  $\epsilon \rightarrow 0$ , it then follows

$$f = (\theta_1 \theta_2 + a_{12}) l_1 l_2 + (\theta_1 \theta_2 + a_{12} + a_{13} \theta_2 + a_{23} \theta_1 + a_{13} a_{23}) l_1 l_2 e^{\eta_3}, \tag{22}$$

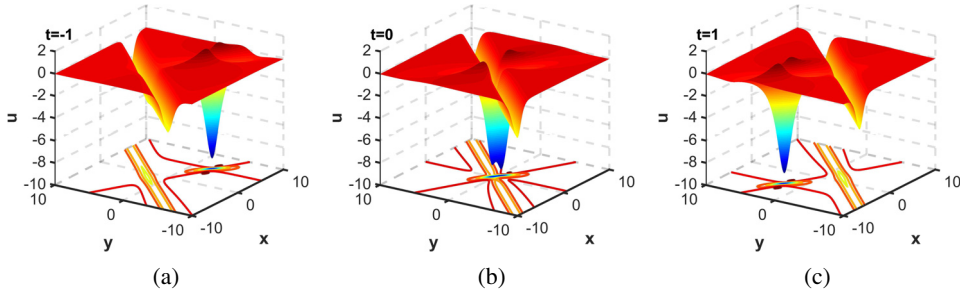


Fig. 10. (Color online) Elastic collision of dark soliton and dark lump in the  $(x, y)$  plane. Parameters are given in Eq. (24) and the other planes have similar process.

where

$$\begin{aligned} \theta_i &= x + p_i y + q_i z + \frac{3q_i t}{2p_i}, \\ a_{ij} &= -\frac{2p_j p_i (p_i + p_j)}{(p_i - p_j)(p_i q_j - p_j q_i)}, \\ a_{i3} &= -\frac{2p_3 p_i (p_i + p_3) k_3}{q_3 p_i^2 + (k_3^2 p_3 - q_i - q_3) p_3 p_i + p_3^2 q_i} \quad (i = 1, 2). \end{aligned} \quad (23)$$

Let

$$p_1 = p_2^* = 1 + I, \quad q_1 = q_2^* = 3 + I, \quad p_3 = 2, \quad q_3 = 1, \quad \eta_3^0 = 0, \quad k_3 = 2. \quad (24)$$

We derive interaction solution of Eq. (1) in the  $(x, y)$  plane, whose dynamical behavior is plotted in Fig. 10. It is clear that the lump and the soliton are dark states. During the propagation, the collision between them is elastic. With a shifting of  $t$ , the patterns of the dark soliton and the dark lump do not change. At  $t = 0$ , the peak and valley of the dark lump solution are divided by the dark soliton.

In the case of  $N = 4$ , similar with the above two cases, assuming

$$k_1 = l_1 \epsilon, \quad k_2 = l_2 \epsilon, \quad k_3 = l_3 \epsilon, \quad k_4 = l_4 \epsilon, \quad \eta_1^0 = \eta_2^{0*} = \eta_3^0 = \eta_4^{0*} = I\pi, \quad (25)$$

it follows

$$\begin{aligned} f &= (\theta_1 \theta_2 \theta_3 \theta_4 + a_{12} \theta_3 \theta_4 + a_{13} \theta_2 \theta_4 + a_{14} \theta_2 \theta_3 + a_{23} \theta_1 \theta_4 + a_{24} \theta_1 \theta_3 \\ &\quad + a_{34} \theta_1 \theta_2 + a_{12} a_{34} + a_{13} a_{24} + a_{14} a_{23}) l_1 l_2 l_3 l_4 \epsilon^4 + O(\epsilon^5), \end{aligned} \quad (26)$$

where

$$\begin{aligned} \theta_i &= x + p_i y + q_i z + \frac{3q_i t}{2p_i}, \\ a_{ij} &= -\frac{2p_i p_j (p_i + p_j)}{(p_i - p_j)(p_i q_j - p_j q_i)} \quad (i, j = 1, 2, 3, 4). \end{aligned} \quad (27)$$

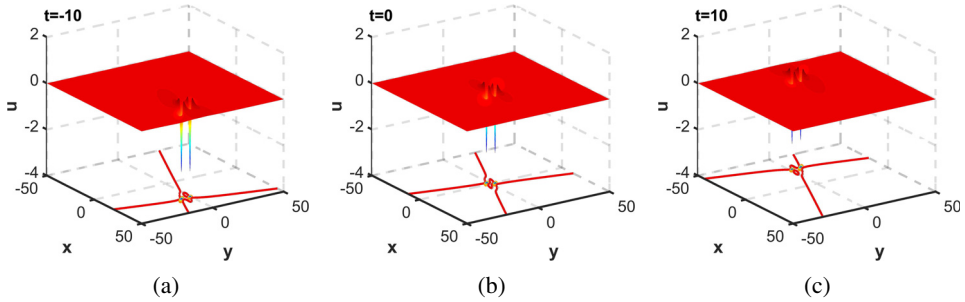


Fig. 11. (Color online) Elastic collision of two dark lumps in the  $(x, y)$  plane. Parameters are constrained in Eq. (29) and (a)  $t = -10$ , (b)  $t = 0$  and (c)  $t = 10$ .

Let

$$\begin{aligned}
 p_1 = p_2^* &= a_1 + Ib_1, & p_3 = p_4^* &= a_2 + Ib_2, \\
 q_1 = q_2^* &= c_1 + Id_1, & q_3 = q_4^* &= c_2 + Id_2,
 \end{aligned}
 \tag{28}$$

where  $a_i, b_i, c_i, d_i$  ( $i = 1, 2$ ) are all real constants. Different interaction solutions in different planes can be derived with the choices of appropriate parameters. Without loss of generality, setting

$$a_1 = 1, \quad b_1 = 1, \quad a_2 = 1, \quad b_2 = 2, \quad c_1 = 2, \quad d_1 = 1, \quad c_2 = 2, \quad d_2 = 3, \tag{29}$$

two-order dark lump can be derived. Dynamical behavior in the  $(x, y)$  plane is visually shown in Fig. 11. Both three dimensions and projected images are plotted to exhibit the dynamical characteristics. Obviously, the two-order dark lump solution keeps permanent lump state with the development of time.

### 2.4. The rogue wave solution

In this part, we can not only construct lump solutions, but also the rogue wave solutions with the long wave limit method on the soliton solution. Now, we will give out the detailed process of constructing rogue wave solutions and interaction solutions and demonstrate dynamic characteristics.

In the case of  $N = 2$ , when  $b_2 = 0$  in the trajectory Eq. (20), namely  $q_1$  and  $q_2$  are real constants, line rogue wave solutions of Eq. (1) can be obtained. To better demonstrate this phenomenon, we constraint the parameters as constructing the lump solutions. For instance, when  $a_1 = 1, b_1 = 2, a_2 = 2, b_2 = 0$ , line rogue wave is constructed in  $(x, z)$  plane. It comes from a constant background and disappears in the infinity. The amplitude reaches maximum 9.6 at  $t = 0$ . The dynamic behavior can be seen in Fig. 12. In the case of  $N = 3$ , by assuming  $p_1 = p_2^* = 1 + I, q_1 = q_2 = 3, p_3 = q_3 = -1, \eta_3^0 = 0, k_3 = 2$ , interaction solution between dark soliton and line rogue wave will be generated in  $(x, z)$  plane. The dynamic features of the interaction solution are exhibited in Fig. 13.

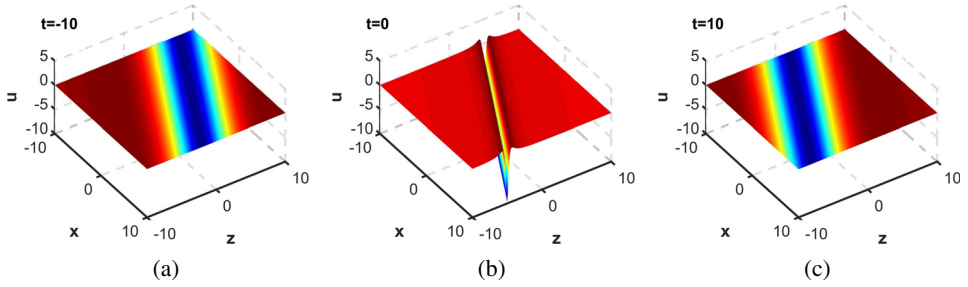


Fig. 12. (Color online) Line rogue waves (18) with  $a_1 = 1$ ,  $b_1 = 2$ ,  $a_2 = 2$ ,  $b_2 = 0$  at  $y = 0$ .

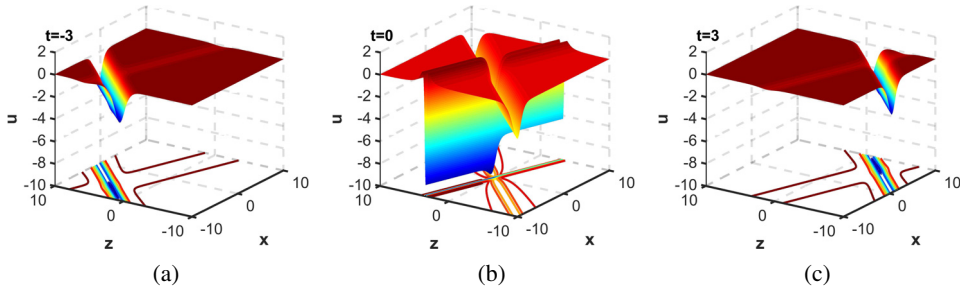


Fig. 13. (Color online) Collision of dark soliton and line rogue wave in the  $(x, z)$  plane at  $y = 0$ .

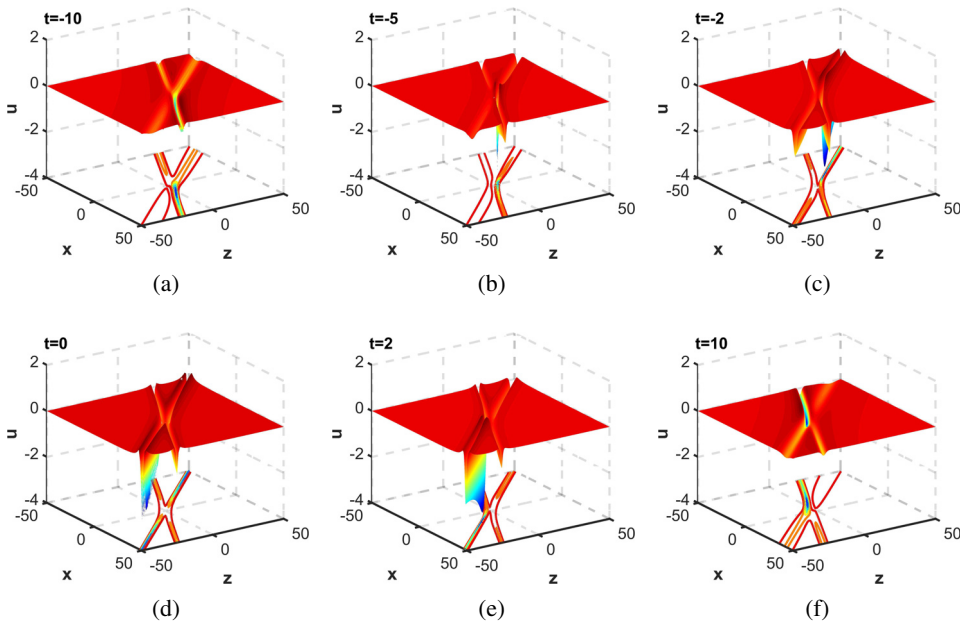


Fig. 14. (Color online) Two line rogue waves in the  $(x, z)$  plane with  $a_1 = 1$ ,  $b_1 = 1$ ,  $a_2 = 3$ ,  $b_2 = 2$ ,  $c_1 = 1$ ,  $c_2 = 2$ ,  $d_1 = d_2 = 0$  at  $y = 0$ .

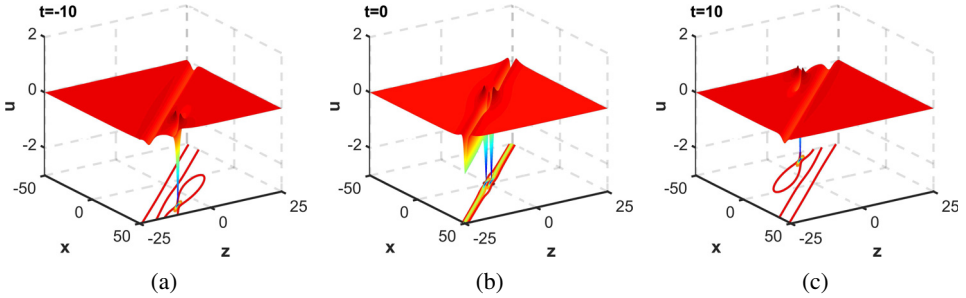


Fig. 15. Collision between line rogue wave and dark lump in the  $(x, z)$  plane with  $a_1 = 1, b_1 = 1, a_2 = 3, b_2 = 2, c_1 = 2, d_1 = 1, c_2 = 2, d_2 = 0$  at  $y = 0$ .

In the case of  $N = 4$ , two kinds of interaction solutions can be obtained by selecting distinct parameters. When  $a_1 = 1, b_1 = 1, a_2 = 3, b_2 = 2, c_1 = 1, c_2 = 2, d_1 = d_2 = 0$ , two line rogue waves could be obtained in  $(x, z)$  plane. Dynamic phenomena are clearly plotted in Fig. 14, which are similar with the above single line rogue wave and amplitude is up to the maximum 2.7079 at  $t = 0$  in Fig. 14(c).

When  $a_1 = 1, b_1 = 1, a_2 = 3, b_2 = 2, c_1 = 2, d_1 = 1, c_2 = 2, d_2 = 0$ , another interaction solution between dark lump and line rogue wave is derived in the  $(x, z)$  plane. To demonstrate their collision process more intuitively, the related graphs for this interaction solution can be seen in Fig. 15. The process of their collision is similar to the collision between dark soliton and line rogue wave.

### 3. Summary and Discussion

In summary, four kinds of localized wave solutions of the  $(3 + 1)$ -dimensional nonlinear evolution equation are investigated in this paper. By the Hirota bilinear method,  $N$ -soliton solutions are constructed and the plots of one, two and three dark solitons in the  $(x, t)$  plane are given (see Fig. 1). By the complex conjugate method on soliton solutions, breathers, interaction solutions between breathers and solitons are obtained in six different planes. General breathers (see Fig. 2), line breathers (see Fig. 3), interaction solutions between dark soliton and line breather (see Fig. 4) or general breather (see Fig. 5) and two-order breathers (see Figs. 6–8) are obtained, respectively. Line breathers are periodic line waves and periodic in both  $x$ - and  $z$ -directions, while general breathers are periodic in one direction and localized in another direction. By the long wave limit method, lumps and rogue waves are derived with the same constrained parameters. Three types of solutions related with lumps are exhibited in this paper, including dark lumps (see Fig. 9) in six different planes, interaction solutions between dark solitons and dark lumps (see Fig. 10) in the  $(x, y)$  plane, interaction solutions between two dark lumps (see Fig. 11) in the  $(x, y)$  plane. The dark lumps are localized in all directions. With the same method, three types of solutions related with rogue waves are also exhibited in the  $(x, z)$  plane, including line rogue wave (see Fig. 12), interaction solution

between dark soliton and line rogue wave (see Fig. 13), interaction solution between two line rogue waves (see Fig. 14), interaction solution between dark lump and line rogue wave (see Fig. 15).

## Acknowledgments

The project is supported by the Global Change Research Program of China (No. 2015CB953904), National Natural Science Foundation of China (Nos. 11675054 and 11435005), and Shanghai Collaborative Innovation Center of Trustworthy Software for Internet of Things (No. ZF1213).

## References

1. X. G. Geng, *J. Phys. A: Math. Gen.* **36** (2003) 2289.
2. X. G. Geng and Y. L. Ma, *Phys. Lett. A* **369** (2007) 285.
3. Zhaqilao and Z. B. Li, *Mod. Phys. Lett. B* **22** (2008) 2945.
4. M. G. Asaad and W. X. Ma, *Appl. Math. Comput.* **219** (2012) 213.
5. Zhaqilao, *Phys. Lett. A* **377** (2013) 3021.
6. Z. L. Zhao, Y. F. Zhang and W. J. Rui, *Appl. Math. Comput.* **248** (2014) 456.
7. A. M. Wazwaz, *Chaos Soliton. Fract.* **76** (2015) 93.
8. A. M. Wazwaz, *Proc. Romanian Acad. Ser. A* **16** (2015) 32.
9. A. M. Wazwaz, *Math. Methods Appl. Sci.* **39** (2016) 886.
10. H. Z. Liu, X. Q. Liu, Z. G. Wang and X. P. Xin, *Nonlinear Dynam.* **85** (2016) 281.
11. M. T. Darvishi, L. Kavitha, M. Najafi and V. S. Kumar, *Nonlinear Dynam.* **86** (2016) 765.
12. N. Liu and Y. S. Liu, *Comput. Math. Appl.* **71** (2016) 1645.
13. Y. N. Tang, S. Q. Tao, M. L. Zhou and Q. Guan, *Nonlinear Dynam.* **89** (2017) 429.
14. H. Q. Zhang and W. X. Ma, *Comput. Math. Appl.* **73** (2017) 2339.
15. Y. B. Shi and Y. Zhang, *Commun. Nonlinear Sci.* **44** (2017) 120.
16. Y. H. Yin, W. X. Ma, J. G. Liu and X. Lü, *Comput. Math. Appl.* **76** (2018) 1275.
17. Y. Zhang, Y. P. Liu and X. Y. Tang, *Comput. Math. Appl.* **76** (2018) 592.
18. J. C. Pu and H. C. Hu, *Appl. Math. Lett.* **85** (2018) 77.
19. C. Rogers and W. K. Schief, *Bäcklund and Darboux Transformations: Geometry and Modern Applications in Soliton Theory* (Cambridge University Press, Cambridge, 2002).
20. M. J. Ablowitz and P. A. Clarkson, *Solitons, Nonlinear Evolution Equations and Inverse Scattering* (Cambridge University Press, Cambridge, 1991).
21. M. J. Ablowitz, D. J. Kaup, A. C. Newell and H. Segur, *Stud. Appl. Math.* **53** (1974) 249.
22. V. B. Matveev and M. A. Salle, *Darboux Transformations and Solitons* (Springer, Berlin, 1991).
23. C. H. Gu, H. S. Hu and Z. X. Zhou, *Darboux Transformation in Soliton Theory and Its Geometric Applications* (Shanghai Scientific and Technical Publishers, Shanghai, 1999).
24. G. W. Bluman and S. C. Anco, *Symmetry and Integration Methods for Differential Equations* (Springer, New York, 2002).
25. P. J. Olver, *Application of Lie Group to Differential Equation* (Springer, New York, 1986).
26. S. Y. Lou, X. R. Hu and Y. Chen, *J. Phys. A: Math. Theor.* **45** (2012) Article 155209.

27. J. C. Chen and Z. Y. Ma, *Appl. Math. Lett.* **64** (2017) 87.
28. Y. H. Wang and H. Wang, *Nonlinear Dynam.* **89** (2017) 235.
29. L. L. Huang and Y. Chen, *Appl. Math. Lett.* **64** (2017) 177.
30. L. L. Huang and Y. Chen, *Nonlinear Dynam.* **92** (2018) 221.
31. L. L. Huang and Y. Chen, *Commun. Nonlinear Sci.* **67** (2019) 237.
32. R. Hirota, *The Direct Method in Soliton Theory* (Cambridge University Press, Cambridge, 2004).
33. W. X. Ma and E. G. Fan, *Comput. Math. Appl.* **61** (2011) 950.
34. C. S. Gardner, J. M. Greene, M. D. Kruskal and R. M. Miura, *Phys. Rev. Lett.* **19** (1967) 1095.
35. X. Wang and L. Wang, *Comput. Math. Appl.* **75** (2018) 4201.
36. K. Imai, *Prog. Theor. Phys.* **98** (1997) 1013.
37. D. J. Kaup, *J. Math. Phys.* **22** (1981) 1176.
38. W. X. Ma, *Phys. Lett. A* **379** (2015) 1975.
39. M. J. Dong, S. F. Tian, X. W. Yan and L. Zou, *Comput. Math. Appl.* **75** (2018) 957.
40. H. Q. Zhang, J. S. Geng and M. Y. Zhang, *Mod. Phys. Lett. B* **32** (2018) 1850334.
41. Y. Q. Liu and X. Y. Wen, *Mod. Phys. Lett. B* **32** (2018) 1850161.
42. D. J. Kedziora, A. Ankiewicz and N. Akhmediev, *Phys. Rev. E* **85** (2012) 066601.
43. M. Tajiri and T. Arai, *Phys. Rev. E* **60** (1999) 2297.
44. C. Liu, Z. Y. Yang, L. C. Zhao and W. L. Yang, *Phys. Rev. A* **89** (2014) 055803.
45. J. C. Chen, B. F. Feng, K.-I. Maruno and Y. Ohta, *Stud. Appl. Math.* **141** (2018) 145.
46. N. Akhmediev, J. M. Soto-Crespo and A. Ankiewicz, *Phys. Rev. A* **80** (2009) 043818.
47. A. Chabchoub, N. P. Hoffmann and N. Akhmediev, *Phys. Rev. Lett.* **106** (2011) 204502.
48. L. Draper, *Marine Observer* **35** (1965) 193.
49. D. R. Solli, C. Ropers, P. Koonath and B. Jalali, *Nature* **450** (2007) 1054.
50. D. A. G. Walker, P. H. Taylor and R. E. Taylor, *Appl. Ocean Res.* **26** (2005) 73.
51. B. Kibler, J. Fatome, C. Finot, G. Millot and F. Dias, *Nat. Phys.* **6** (2010) 790.
52. Y. Ohta and J. K. Yang, *Phys. Rev. E* **86** (2012) 036604.
53. B. L. Guo, L. M. Ling and Q. P. Liu, *Phys. Rev. E* **85** (2012) 026607.
54. Z. Y. Yan, *Phys. Lett. A* **375** (2011) 4274.
55. J. S. He, H. R. Zhang, L. H. Wang and A. S. Fokas, *Phys. Rev. E* **87** (2013) 052914.
56. L. M. Ling and L. C. Zhao, *Phys. Rev. E* **88** (2013) 043201.
57. X. Wang, C. Liu and L. Wang, *J. Math. Anal. Appl.* **449** (2017) 1534.
58. N. Akhmediev and V. I. Korneev, *Theor. Math. Phys.* **69** (1986) 1089.
59. Y. C. Ma, *Stud. Appl. Math.* **60** (1979) 73.
60. J. G. Rao, Y. Cheng and J. S. He, *Stud. Appl. Math.* **139** (2017) 568.
61. C. Qian, J. G. Rao, Y. B. Liu and J. S. He, *Chinese Phys. Lett.* **33** (2016) 110201.
62. Y. F. Yue, L. L. Huang and Y. Chen, *Comput. Math. Appl.* **75** (2018) 2538.
63. L. L. Huang, Y. F. Yue and Y. Chen, *Comput. Math. Appl.* **76** (2018) 831.
64. Y. F. Yue, L. L. Huang and Y. Chen, *Appl. Math. Lett.* **89** (2019) 70.
65. M. J. Ablowitz and J. Satsuma, *J. Math. Phys.* **19** (1979) 2180.
66. J. Satsuma and M. J. Ablowitz, *J. Math. Phys.* **20** (1979) 1496.